PNAS
www.pnas.org

Supplementary Information for

N-acyl taurines are endogenous lipid messengers that improve glucose homeostasis

Trisha J. Grevengoed, Samuel A.J. Trammell, Michele K. McKinney, Natalia Petersen, Rebecca L. Cardone, Jens S. Svenningsen, Daisuke Ogasawara, Christina C. Nexøe-Larsen, Filip K. Knop, Thue W. Schwartz, Richard G. Kibbey, Benjamin F. Cravatt, Matthew P. Gillum

Corresponding author: Matthew P. Gillum
Email: gillum@sund.ku.dk

This PDF file includes:

Supplementary text
Figures S1 to S3
SI References

www.pnas.org/cgi/doi/10.1073/pnas.1916288116

Supplementary Information Text

MATERIALS AND METHODS

Generation of FAAH-S268D knock-in mice

The FAAH gene was obtained from a 129SvJ BAC library and used as a template for cloning. A 3.0 kb region encompassing exons 3-7 was amplified with the following primers:

Primer C, 5'- GGCCGCGGTCCAACTGATATCATTCCTTCTAGGC
Primer D, 5'- GCCCGCGGGGTGGTCCTCTGCAGCTAGGG

This region was then subcloned and the S268D mutation introduced by site-directed mutagenesis. A second 3.0 kb region encompassing exons 8-11 was amplified with the following primers:

Primer E, 5'- CAGAATTCCCGCAGTCTCTGCTCCCATGCCAGC
Primer F, 5'- CCCATATGAAGCTTCAGGGCCCCACCTGATGGC

An FRT-flanked PGK-Neo cassette (gift from Ulrich Mueller), consisting of a phosphoglycerate kinase promoter driving the neomycin phosphotransferase gene, was then inserted between exons 7 and 8. This construct comprising exons 3-11, the S268D point mutation, and the PGK-Neo cassette, was microinjected into 129SvJ embryonic stem cells. Homologously recombined embryonic stem cell clones were identified by Southern analysis, with an external probe located 5' of the targeted region. The 5' probe gave differential band sizes in WT (8.0 kb) or targeted (4.0 kb) genomic DNA digested with SacI. One homologous recombinant was identified expanded and injected into albino C57BL/6 blastocysts. Blastocysts were implanted into pseudopregnant albino C57BL/6 females generate chimeric males. 12 chimeras produced germ-line transmission of the targeted mutation, which was confirmed by Southern analysis.

Sequencing to confirm the S268D knockin mutation within the mouse line was performed using genomic tail DNA. Genomic DNA from a FAAH-WT, FAAH-WT/S268D, and FAAH-S268D/S268D mice were sequenced utilizing the following primers which ended on the mutation:

Mutation PCR screen forw: 5'- CAAGAGTGGCCTGAAG**AG**
Mutation PCR screen rev: 5'- CTGCTGTCTGTCCATAAACACA**GCT**

Further confirmation sequencing was performed with primers approximately 270 bp up and downstream from the mutation:

Mutation PCR screen forw270: 5'- AGCCTACTGG
Mutation PCR screen rev270: 5'- AGAAAGCTGC

Utilizing the FRT-flanked PGK-Neo cassette, heterozygous S268D-FAAH knock-in mice were bred with 129S4/SvJaeSor-Gt(ROSA)$^{26Sortm1(FLP1)Dym}$/J mouse (Jax Cat #003946). FLP-mediated recombination then resulted in deletion of the *frt*-flanked sequence(s) in the offspring.

PCR genotyping of genomic tail DNA was performed to confirm the loss of neo cassette using the following primers:

S268D primer WT Rev 5' – CAACTCCTGGTTGAAAGATCC
S268D primer WT Forw 5' – GTGAGGATTTGTTCCGCTTGG
S268D primer KI Rev 5' – AATAAGAACTTCGGCCGCCACC

These primers amplify a 475- and a 240-bp product from WT and knock in mouse, respectively.

Heterozygotic mice were then backcrossed for at least five generations onto a C57Bl/6 background and intercrossed to furnish homozygotic FAAH-S268D mice.

Sample preparation for NAT analyses

Human plasma was obtained from 4 female subjects, mean age 54.3 after gallbladder removal. The study was approved by the Regional Committee of Copenhagen area (Den Videnskabsetiske Komite F for Region Hovedstaden, H-15016324). The subjects gave informed consent prior to any trial activity. Standard quality controls (Std QCs), calibrants, and samples were dosed with 5 pmol of internal standard (C15:0 NAT) prior to extraction. 150 µL of EDTA-produced plasma resting on ice was extracted as described (1) with two slight modifications. 1) 80% methanol containing 2.5 mM triethylammonium acetate was used instead of 75% methanol. 2) Only the organic (ether) phase was dried using a Gene Vac EZ 2 until void of solvent instead of a mixture of aqueous and organic phases. Standard QCs (Std QC) (final concentrations: 0.125, 0.625, and 1.25 µM of C18:0 and C18:1 NAT) and calibrants (final concentrations: 0, 0.025, 0.05, 0.1, 0.25, 0.3, 0.6, 0.5, 0.75, 1, 1.5, 2 µM µM of C18 and C18:1 NAT) were composed by adding 10 µL of standard to LCMS water. Std QCs were composed in the presence of either water or human plasma from an unrelated cohort in triplicate at the same concentrations as above. An unadulterated, human plasma sample was also processed to serve as a blank. A blank containing only internal standard and a blank containing only extraction solvent were also prepared. All Std QCs, calibration points, and blanks were extracted in the same manner as samples. In experiments wherein mice received an injection of C18:1 NAT, the concentrations of QCs and calibration points were increased by 10 fold. All samples were suspended with vigorous pipetting and brief vortexing (~3 s, top speed) in 50 µL of 2-propanol/acetonitrile/water (2:1:1 v/v/v) while resting on wet ice. 45 µL of centrifuged (20,238 x g, 22 °C, 10 min) sample was transferred to a fresh autosampler vial. Equal volumes of all samples were pooled into one vial to compose the QC pool. Sample order was randomized prior to analysis. All were stored in a prechilled (8 °C) Dionex Ultimate 3000 autosampler throughout analysis.

Liquid chromatography-mass spectrometry (LC-MS) for NAT quantification

10 µL of sample was separated using chromatography as described (2) with slight modification. Mobile phase A and B were changed to 1 mM acetic acid in water and 1 mM acetic acid in acetonitrile/2-propanol (1:9 v/v), respectively. This alteration increased signal in negative ion mode by approximately 2-fold in agreement with previous studies in negative ion mode (3). The gradient was altered with a hold at 60% A for 2 min. The rest of the gradient was unaltered. In the beginning of each sequence, two solvent blanks and six QC pool injections were performed to equilibrate the system. In all cases, the QC pool and Std QCs were injected at equal intervals throughout the queue to ensure reproducibility.

Before beginning analysis, the instrument was calibrated by directly infusing sodium acetate. Calibration was modeled with HPC mode. Calibrant was also infused at the beginning of each analysis. Calibration was further improved by infusing a lock mass (0.1 mg/mL hexakis (1H, 1H, 2H-perfluoroethoxy) phosphazene in 2-propanol). Analytes ionized via electrospray were detected in full scan (*m/z*: 50 – 1000), negative ion mode with a Bruker Impact II Q-TOF. The instrument was operated using the following conditions: cone voltage = 30 kV, collision energy = 25 eV (optimized for NATs), nebulizer gas flow = 10 L/h, nebulizer gas temperature = 220 C, nebulizer pressure = 2 bar, and a scan rate = 2 Hz.

C18:0 (*m/z*: 390.2685, retention time (RT) = 5.6 min) and C18:1 (*m/z*: 388.2525, RT = 4.9 min) NAT areas were converted to pmol amounts using a weighted (1/x), internally controlled standard curve. Micromolar concentrations were determined by dividing the pmol amounts by the extracted sample volume and correcting for percent loaded. R^2 values of greater than 0.998 were considered valid curves. Any standard deviating by more than 20% of the theoretical value was excluded. A standard curve was considered valid if greater than 75% of the calibration curves points deviated by less than or equal to 20%.

Raw files were converted to .cdf format and analyzed using XCMS Online (4). Features were detected using the centwave method with a mass tolerance of 10 ppm, minimum peak width of 5, maximum peak width of 20, signal-to-noise of 6, mzdiff of 0.01, integration method 1, prefilter peaks of 3, prefilter intensity of 100, and noise filter of 100. Features were grouped with the following parameters: bw of 5, minfrac of 0.5, mzwid of 0.015, minsamp of 1, and max of 100. Retention times were corrected using the obiwarp method with a step size of 1. In the comparison of wildtype and FAAH-S268D mice, the resulting output was further analyzed using MetaboAnalyst 3.0 (5) after filtering away features eluting before 1 min. Data were normalized to row-wise sum intensity, $\log_2$ transformed and Pareto scaled. Differentially regulated features were visually inspected in the raw data. Features of poor peak shape or isotopic features were discarded from further analysis. All remaining features were fragmented using LC-MS/MS. Features producing taurine (m/z: 124.0074) and fragments related to taurine (m/z: 79.9574 and 106.9808) were deemed NATs. In experiments in which no comparison was warranted, EICs were generated for the following NATs: C16:0 (*m/z*: 362.2371, RT = 4.69 min) C16:1 (*m/z*: 360.2214, RT = 3.28 min), C16:2 (*m/z*: 358.2057, RT = 2.36 min), C18:0 (as above), C18:1 (as above), C18:2 (*m/z*: 386.2370, RT = 4.1 min), C18:3 (*m/z*: 384.2213, RT = 3.3 min), C20:3 (*m/z*: 412.2527, RT = 4.7 min), C20:4 (*m/z*: 410.2369, RT = 4.22 min), C20:5 (*m/z*: 408.2212, RT = 3.22 min), C22:0 (*m/z*: 446.3311, RT = 6.85 min), C22:6 (*m/z*: 434.2367, RT = 4.22 min), and C24:6 (*m/z*: 462.2683, RT = 5.08 min).
Quantities were estimated using the following expression:

$$C * \frac{If}{Io}$$

where *C* is the concentration of C18:1 NAT in the sample, *If* is the intensity of the feature within the sample, and *Io* is the intensity of C18:1 NAT within the sample.

Preparation of tissue proteomes
Mouse livers were dounce-homogenized in cold DPBS and the homogenates were subjected to low-speed spin (1,400 x *g*, 3 min, 4°C) to remove debris. The resulting supernatant was subjected to high-speed spin (100,000 x *g*, 45 min, 4°C) to separate membrane and cytosolic fractions. The resulting membrane pellet was washed with cold DPBS and resuspended with cold DPBS. Total protein concentrations of membrane fractions were determined using the Bio-Rad DC protein assay kit.

Western blot
25 µg of protein for each liver lysate were separated by SDS-PAGE and then transferred to a PVDF membrane in Towbin buffer. The membrane was blocked using 5% nonfat dry milk (w/v) in Tris-buffered saline with Tween 20 (TBST) for 1 h at room temperature and incubated with anti-FAAH antibody (Cell Signaling, 1:1000 dilution in 5% nonfat dry milk in TBST) overnight at 4°C or anti-GAPDH antibody (Santa Cruz, 1:1000 dilution in 5% nonfat dry milk in TBST) for 1 h at room temperature. Blots were washed (5 min x 3 times) with TBST, incubated with HRP-conjugated anti-mouse secondary antibody (Bio-Rad, 1:3000 in 5% nonfat dry milk in TBST) for 1 h at room temperature and washed (5 min x 3 times) with TBST. Protein-antibody complexes were visualized by enhanced chemiluminescence (ECL, Thermo Fisher) imaged on the ChemiDoc Imaging System (Bio-Rad).

Proteomic analysis of liver membrane lysate
2 mg of liver membrane proteomes (2 mg/mL in DPBS) were incubated with 5 µM FP-biotin for 1 h at room temperature, and the proteomes were denatured followed by precipitation using 4:1 MeOH/$CHCl_3$ (v/v). The precipitates were subject to reduction, alkylation, avidin-based enrichment, and on-bead trypsin digestion. The digested peptides were subjected to reductive dimethylation as previously described (6, 7). Briefly, formaldehyde (light) or ^{13}C-labeled deuterated formaldehyde (heavy) was added to the liver membrane proteome from FAAH (WT/WT) or FAAH (S268D/ S268D) mice respectively (0.2%, w/v) followed by the addition of sodium cyanoborohydride (27 mM final concentration). After 2 h of incubation, the reaction was quenched by the addition of NH_4OH (0.2% final concentration, v/v) and formic acid (8% final

concentration, v/v). The light- and heavy-labeled samples were then combined and analyzed by LC/MS analysis as described previously (8–11).

Rat islet reaggregate insulin and glucagon secretion

Rat islets were isolated from Sprague-Dawley rats and recovered in culture at 37^{o}C 5% CO_2/95% for 12-24hrs in 5 mM glucose RPMI supplemented with 10 mM HEPES, 10% fetal bovine serum and antibiotics. The islets were then dispersed and re-aggregated into pseudo islets as described for human islets. Rat islet cells were treated identically except for incubation in DMEM in place of Krebs-Ringer buffer.

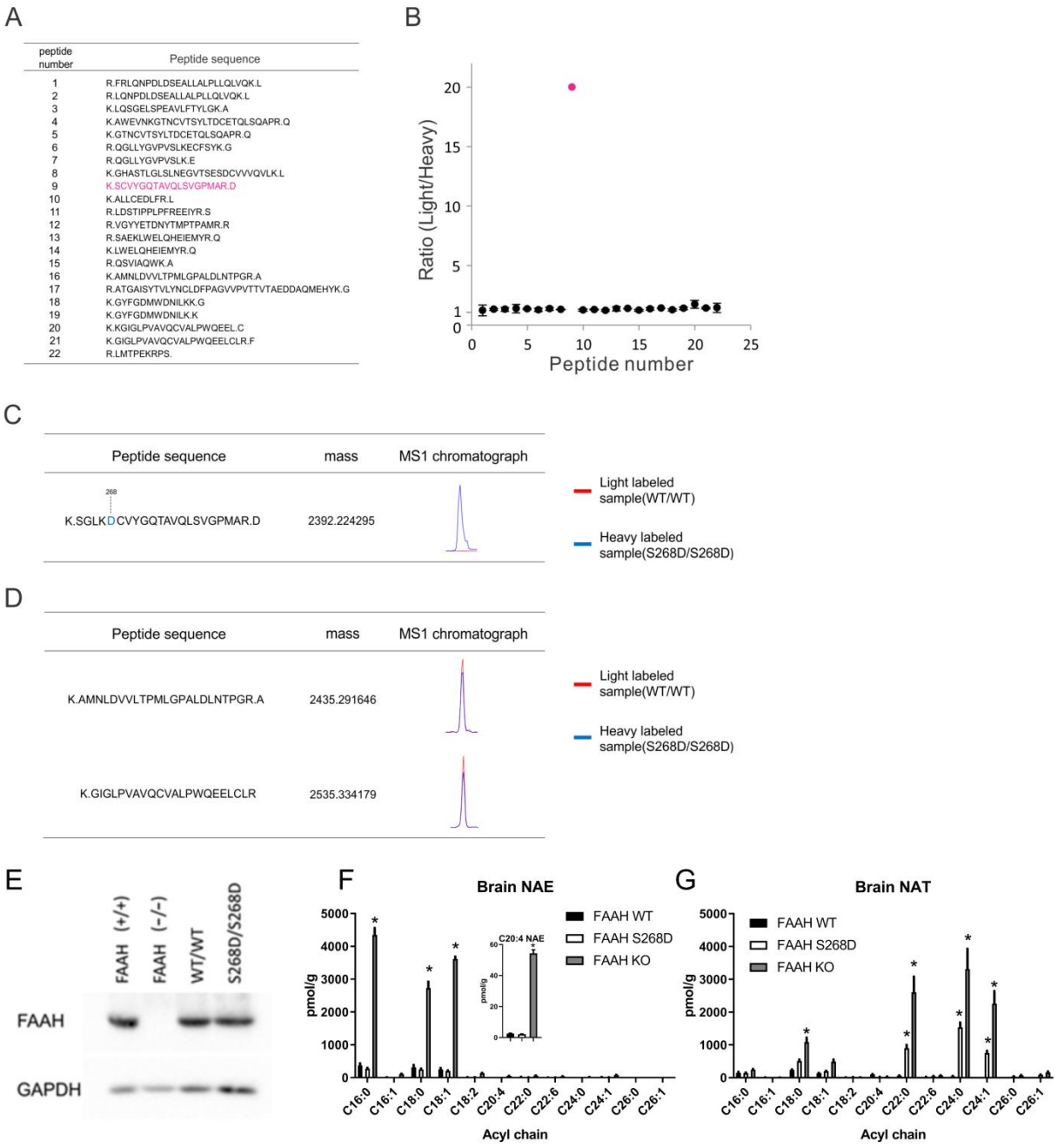

Fig. S1. Chemoproteomic analysis of liver membrane lysates from FAAH (WT/WT) and FAAH (S268D/S268D) mice. A) List of detected FAAH peptide sequences. B) Dot plot of Light (WT/WT)/Heavy (S268D/S268D) ratio of the FAAH peptides shown in (A). Ratio represents mean ± SD of the median ratio of each peptide from 2 biological replicates. The S268 containing peptide was marked as red. C) S268D mutant FAAH peptide was detected in FAAH (S268D/S268D) (blue chromatograph) but not in FAAH (WT/WT) (red chromatograph) mouse liver membrane lysate. D) Representative peptides not containing S268 from FAAH (WT/WT) (red chromatograph) and FAAH (S268D/ S268D) (blue chromatograph) mouse liver lysate show similar MS1 intensities. E) Western blot analysis of mouse liver membrane lysate. Brain NATs (F) and NAEs (G) in FAAH-S268D and FAAH KO mice (n=3-4). Data presented as mean ±SEM. *p≤0.05 compared to control.

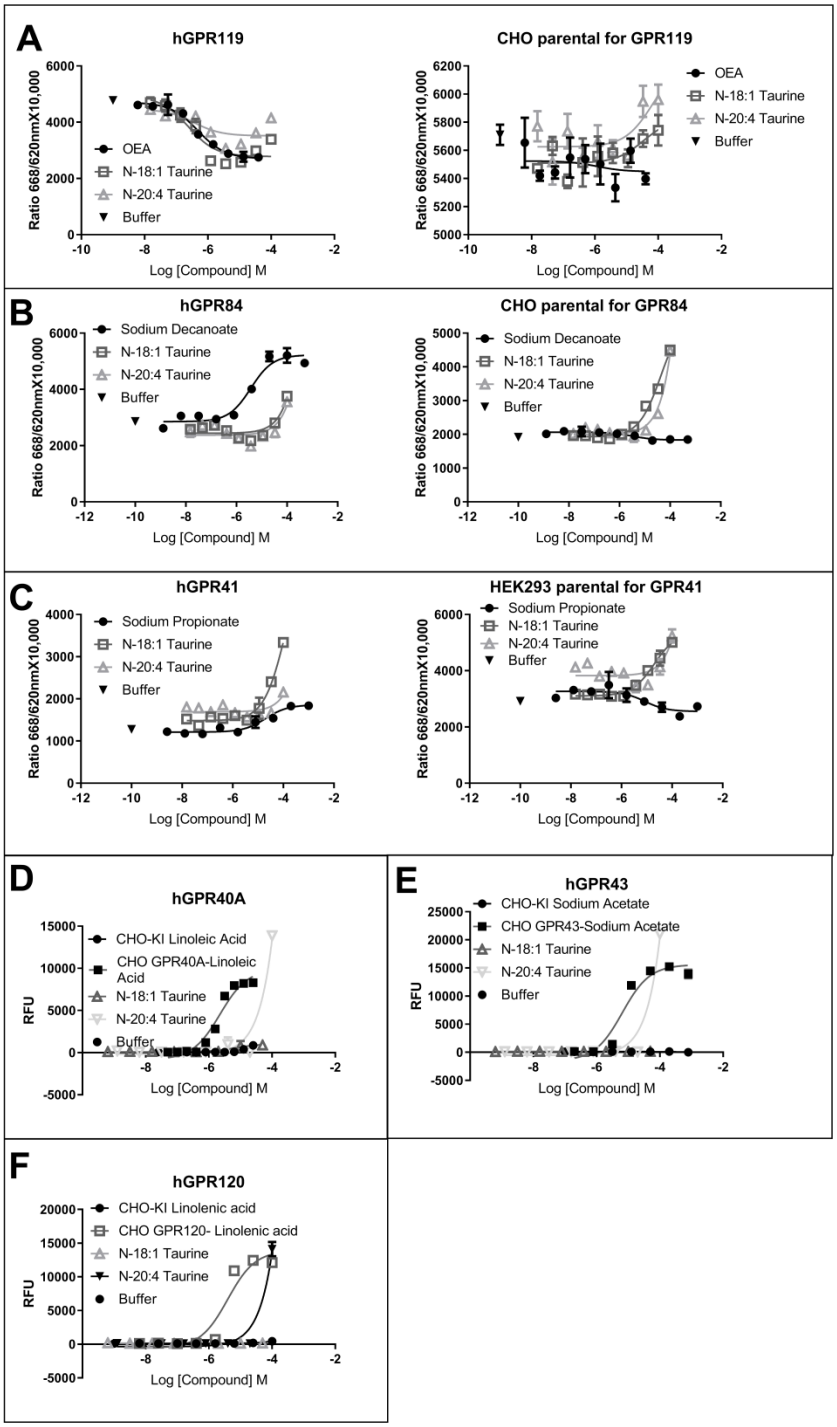

Fig. S2. NAT activation of human FFA GPCRs. A-C) cAMP assay in stably transfected cells treated with NAT or positive control (in triplicate). D-F) Calcium assay in stably transfected cells treated with NAT or positive control (in triplicate).

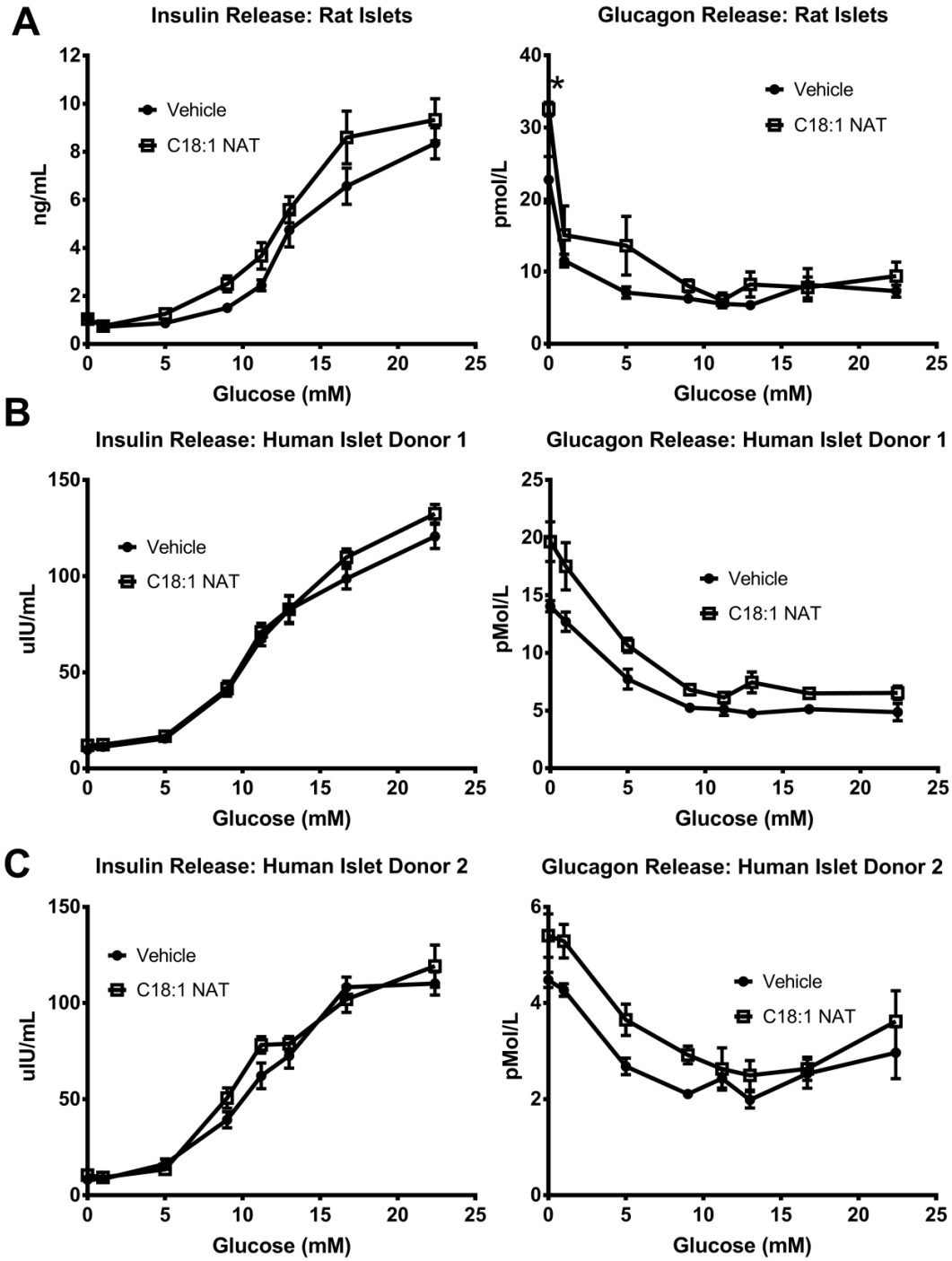

Fig. S3. C18:1 NAT increases glucagon secretion in rat and human islets. A) Insulin and glucagon release in pseudo-islet reaggregates isolated from rat (n=1 in quadruplicate) B-C) Insulin and glucagon release in pseudo-islet reaggregates isolated from humans (individual donors from Fig 5).

References

1. O. Sasso, *et al.*, Endogenous N -acyl taurines regulate skin wound healing. *Proc. Natl. Acad. Sci.* **113**, E4397–E4406 (2016).
2. J. M. Castro-Perez, *et al.*, Comprehensive LC−MS ^{E} Lipidomic Analysis using a Shotgun Approach and Its Application to Biomarker Detection and Identification in Osteoarthritis Patients. *J. Proteome Res.* **9**, 2377–2389 (2010).
3. Z. Wu, *et al.*, Favorable Effects of Weak Acids on Negative-Ion Electrospray Ionization Mass Spectrometry. *Anal. Chem.* **76**, 839–847 (2004).
4. H. Gowda, *et al.*, Interactive XCMS online: Simplifying advanced metabolomic data processing and subsequent statistical analyses. *Anal. Chem.* **86**, 6931–6939 (2014).
5. J. Xia, I. V. Sinelnikov, B. Han, D. S. Wishart, MetaboAnalyst 3.0-making metabolomics more meaningful. *Nucleic Acids Res.* **43**, W251–W257 (2015).
6. D. Ogasawara, *et al.*, Rapid and profound rewiring of brain lipid signaling networks by acute diacylglycerol lipase inhibition. *Proc. Natl. Acad. Sci.* **113**, 26–33 (2015).
7. J. M. Inloes, *et al.*, The hereditary spastic paraplegia-related enzyme DDHD2 is a principal brain triglyceride lipase. *Proc. Natl. Acad. Sci.* **111**, 14924–14929 (2014).
8. J. J. Hulce, A. B. Cognetta, M. J. Niphakis, S. E. Tully, B. F. Cravatt, Proteome-wide mapping of cholesterol-interacting proteins in mammalian cells. *Nat. Methods* **10**, 259–264 (2013).
9. B. R. Martin, C. Wang, A. Adibekian, S. E. Tully, B. F. Cravatt, Global profiling of dynamic protein palmitoylation. *Nat. Methods* **9**, 84–89 (2012).
10. E. Weerapana, *et al.*, Quantitative reactivity profiling predicts functional cysteines in proteomes. *Nature* **468**, 790–797 (2010).
11. M. P. Washburn, D. Wolters, J. R. Yates, Large-scale analysis of the yeast proteome by multidimensional protein identification technology. *Nat. Biotechnol.* **19** (2001).